

2015

# A Southern Hemisphere Sea Level Pressure-Based Precursor for ENSO Warm and Cold Events

B. D. Hamlington


*Old Dominion University*, [bhamling@odu.edu](mailto:bhamling@odu.edu)

R. F. Milliff

H. Van Loon

K.-Y. Kim

Follow this and additional works at: [https://digitalcommons.odu.edu/ccpo\\_pubs](https://digitalcommons.odu.edu/ccpo_pubs)

 Part of the [Atmospheric Sciences Commons](#), [Climate Commons](#), [Meteorology Commons](#), and the [Oceanography Commons](#)

## Repository Citation

Hamlington, B. D.; Milliff, R. F.; Loon, H. Van; and Kim, K.-Y., "A Southern Hemisphere Sea Level Pressure-Based Precursor for ENSO Warm and Cold Events" (2015). *CCPO Publications*. 140.

[https://digitalcommons.odu.edu/ccpo\\_pubs/140](https://digitalcommons.odu.edu/ccpo_pubs/140)

## Original Publication Citation

Hamlington, B.D., Milliff, R.F., Van Loon, H., & Kim, K.Y. (2015). A Southern Hemisphere sea level pressure-based precursor for ENSO warm and cold events. *Journal of Geophysical Research: Atmospheres*, 120(6), 2280-2292. doi: 10.1002/2014JD022674

## RESEARCH ARTICLE

10.1002/2014JD022674

## Key Points:

- CSEOFs are used to extract SLP variability leading to extreme ENSO events
- The dominant Southern Hemisphere CSEOF modes are ENSO related
- SLP variations in May–June–July are shown predict onset of ENSO WE and CE

## Correspondence to:

B. D. Hamlington,  
bhamling@odu.edu

## Citation:

Hamlington, B. D., R. F. Milliff, H. van Loon, and K.-Y. Kim (2015), A Southern Hemisphere sea level pressure-based precursor for ENSO warm and cold events, *J. Geophys. Res. Atmos.*, 120, 2280–2292, doi:10.1002/2014JD022674.

Received 3 OCT 2014

Accepted 17 FEB 2015

Accepted article online 20 FEB 2015

Published online 26 MAR 2015

## A Southern Hemisphere sea level pressure-based precursor for ENSO warm and cold events

B. D. Hamlington<sup>1</sup>, R. F. Milliff<sup>2</sup>, H. van Loon<sup>3</sup>, and K.-Y. Kim<sup>4</sup>

<sup>1</sup>Department of Ocean, Earth and Atmospheric Sciences, Old Dominion University, Norfolk, Virginia, USA, <sup>2</sup>Cooperative Institute for Research in Environmental Sciences, University of Colorado Boulder, Boulder, Colorado, USA, <sup>3</sup>National Center for Atmospheric Research, Boulder, Colorado, USA, <sup>4</sup>School of Earth and Environmental Sciences, Seoul National University, Seoul, South Korea

**Abstract** Past studies have described large-scale sea level pressure (SLP) variations in the Southern Hemisphere that lead to El Niño–Southern Oscillation (ENSO) warm and cold events (WE and CE). By relying on this description and the importance of the related variability in the lead up to WE and CE, Southern Hemisphere SLP variations in May–June–July (MJJ) are shown here to be excellent predictors for the peak warm/cold events in sea-surface temperatures (SST) and sea level pressure that mark the mature phase of a warm/cold event in November–January of the same year. Cyclostationary empirical orthogonal functions (CSEOFs) are used to extract the variability associated with this description of SLP evolution leading to extreme events, underscoring the importance of this signal in the build-up to ENSO events. Using the CSEOF decomposition, an MJJ precursor is established and shown to precede impending warm and cold events in the past sixty years. Furthermore, the precursor developed in this study would have suggested that a significant WE for the latter half of 2014 was unlikely.

### 1. Introduction

The El Niño–Southern Oscillation (ENSO) is an important climate phenomenon centered in the tropical Pacific Ocean with far-reaching effects and near global influence on the Earth System. Dynamically speaking, the warm and cold events of ENSO (WE and CE, respectively), commonly referred to as “El Niño” and “La Niña,” are both manifestations of shifts in the Southern Oscillation (SO) and are not quite a mirror image to each other. Due to the magnitude and scale of its impact, understanding the development and evolution of WE and CE of the SO has been a frequently studied problem, with a range of descriptions presented in the literature over the last several decades [e.g., Bjerknes, 1966, 1969; van Loon and Madden, 1981; Rasmusson and Carpenter, 1982; van Loon and Shea, 1985, 1987; Rasmusson et al., 1990; Latif et al., 1998; Chen et al., 2004; Hong et al., 2014]. In the past, forecasting warm and cold extremes of the SO has largely focused on the equatorial Pacific sea surface temperature (SST) [e.g., Landsea and Knaff, 2000]. The onset of a WE, however, remains difficult to forecast when focusing on equatorial signals alone [Kerr, 2002]. Subtropical and midlatitude processes have been shown to play important roles in the development of extreme events [e.g., van Loon and Shea, 1985; Stephens et al., 2007; Hong et al., 2014]. Longer lead times (e.g., from just after the so-called spring predictability barrier) require a focus on the evolution of the SO and its preconditioning of the tropical Pacific several seasons before tropical triggers (e.g., westerly wind bursts, and eastward advancing Madden-Julian Oscillation active phase convection) lead to the development of tropical SST anomalies associated with the mature WE in the Northern Hemisphere winter.

One particular aspect of the evolution of the SO that posits the onset and development of a WE is the weakening of the South Pacific subtropical high in southern late fall and winter [Bjerknes, 1966, 1969; van Loon, 1984; van Loon and Shea, 1985, 1987; Harrison and Larkin, 1996; Larkin and Harrison, 2002; Kidson and Renwick, 2002; Stephens et al., 2007]. Large-scale shifts in seasonal sea level pressure (SLP) patterns in the Southern Hemisphere midlatitudes precede, by several seasons, the development of a mature WE in the tropics. The seasonal dynamics in the Southern Hemisphere have been described as a 2 year process. The  $year_{-1}$  (year preceding a warm event) and  $year_0$  (year of the warm event) SLP evolution have been described in several of the referenced papers above and subsequently summarized by Stephens et al. [2007]. As discussed in van Loon et al. [2003], an important  $year_0$  precursor signal in the SLP evolution leading to a WE is evident in SLP data from May, June, and July (MJJ) in the Southern Hemisphere midlatitudes. The SLP precursor signal in MJJ for a WE is characterized by anomalous high SLP over Australia and, adjacent to the east, anomalous low SLP

off New Zealand (extending to the south-central Pacific). These SLP anomalies drive seasonal equatorward winds, through the Tasman Sea that are associated with mass build-up in the equatorial western Pacific several months before the mature ENSO tropical SST is evident. As part of this description of the onset of a WE, this Southern Hemisphere SLP evolution in MJJ is a necessary (although not necessarily sufficient) condition for the development of an extreme event at the end of the year. More specifically, the northward anomalous flow between Australia and the central Pacific in MJJ is a necessary precursor, which is not there in February-March-April (FMA). From the perspective of a harmonic (in time) analysis, SLP over Australia has a predominant first harmonic with maxima in MJJ, whereas the SLP over the ocean to the east has a second harmonic with minima in middle latitudes *van Loon* [1967]. Thus, on the average, a northward anomalous flow is found between Australia and the ocean, and the possible condition for a WE is there every year. In some years, the SLP difference is large enough to set off a WE and to carry it into the next season. Additionally, as shown in recent studies [e.g., *Hong et al.*, 2014], this Southern Hemisphere SLP variability plays an important role in the strength of impending ENSO events. Similar but opposite sign patterns can emerge in a CE. Qualitatively, in the context of the discussion here, this is because CEs often result as an over-relaxation from a preceding WE.

Previously, the dynamics of the SLP (and associated signals in wind, convection, and SST) have been described using anomalies and a largely qualitative description without relying on modal analyses [as in *van Loon et al.*, 2003; *Stephens et al.*, 2007]. By separating the SO SLP variability in the Southern Hemisphere into a small number of modes, an MJJ precursor can be developed leading to fewer failed predictions compared to analyses based on anomaly values alone. For example, *Milliff et al.* [2009] demonstrated a method based on time series of area averaged SLP anomalies in the midlatitude South Pacific high-pressure region. Their WE precursor captured only part of the shifting mass in the Southern Oscillation and did not separate effects due to biennial and lower frequency modulations. As such, the area-average SLP anomaly precursor missed 4 of 18 WE in the record since 1948 with no discussion of the effectiveness with regard to CE. While the primary focus of this paper is on the development of the precursor, an important objective is to show how large of a role the MJJ SLP patterns in the Southern Hemisphere play in determining the onset of a WE or CE. The importance of the precursor patterns to be described perhaps suggest a reexamination of current dynamical ENSO forecast models with a renewed focus on SLP variability for long lead times on the Southern Hemisphere.

## 2. Cyclostationary Empirical Orthogonal Function Analysis

To extract the variability associated with SO, a cyclostationary empirical orthogonal function (CSEOF) analysis [*Kim et al.*, 1996; *Kim and North*, 1997] is applied to the monthly average SLP and SST data sets. The CSEOF method decomposes space-time data into a series of modes comprised of a spatial component (known hereafter as the loading vector (LV)) and a corresponding temporal component (known hereafter as the principal component time series (PCTS)). The main difference between CSEOF and the more widely used empirical orthogonal function (EOF) analysis is the LVs' time dependence, which allows the spatial pattern of each CSEOF mode to vary in time, with the temporal evolution of the spatial pattern of the CSEOF LVs constrained to be periodic with a selected "nested period." In other words, the system is defined as

$$\begin{aligned} T(r, t) &= \sum_i LV_i(r, t) PC_i(t) \\ LV(r, t) &= LV(r, t + d) \end{aligned} \quad (1)$$

where the loading vectors are time dependent and are periodic with the nested period,  $d$ . As a result, each CSEOF mode is composed of 12 LVs and 1 PCTS when, for example, using monthly data and a 1 year nested period. In other words, the temporal evolution related to an inherent physical process is captured in the LV, while the corresponding PCTS explains the amplitude of this physical process through time. The nested period of the CSEOF analysis is selected a priori, with the decision usually based on some physical understanding or intuition regarding the data to be studied. When studying the annual signal known to be present in many geophysical data sets, for instance, a nested period of 1 year is chosen. The resulting LV would contain 12 spatial maps (when using monthly data) and would describe the physical evolution of the annual cycle through the year. The PCTS then describes the amplitude change—or strength—of the annual cycle from year to year.

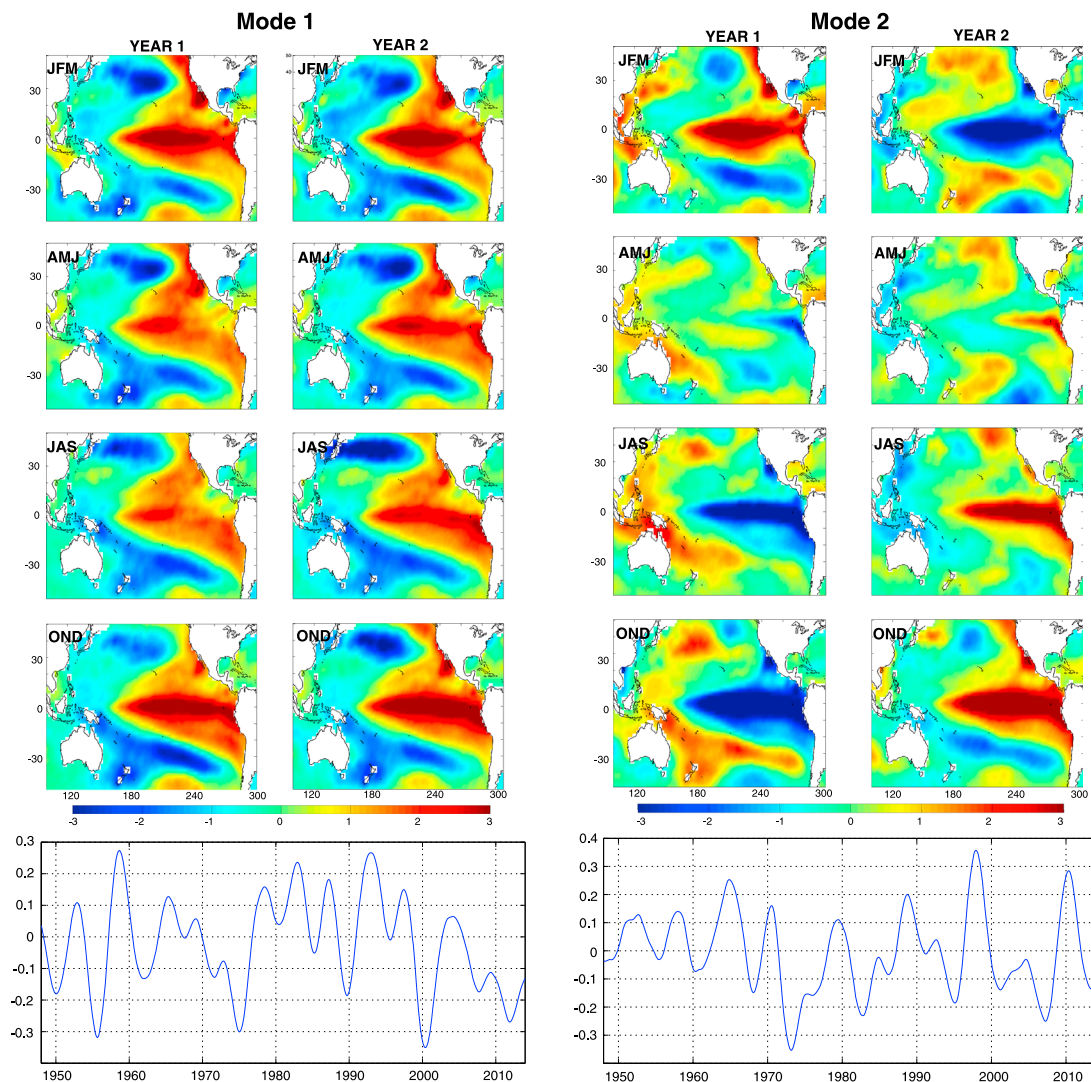


**Figure 1.** (left) Mode 1 (after the seasonal signal and trend are removed) of the CSEOF decomposition of SST data from the ERSSTv3 data set, representing low frequency variability in the northern and tropical Pacific (unit: °C). (top) LVs and (bottom) PCTS are shown. (right) Mode 2 of the CSEOF decomposition of the ERSSTv3 data set, representing the biennial oscillation between warm and cold SO events (unit: °C). Note that 2 year nested period is used.

### 3. CSEOF Analysis of SST

In this study, a nested period of 2 years is selected for the CSEOF decomposition of SST. In general, a 2 year nested period is used for extracting SO-related variability from geophysical data sets. This decision is based primarily on the biennial tendency of the SO [e.g., *Kiladis and van Loon, 1988; Rasmusson et al., 1990*]. Two other studies—*Kim [2002]* and *Yeo and Kim [2013]*—provide a more detailed study of the nested period and established a physical explanation for extracting tropical Pacific Ocean variability with a 2 year nested period. Particularly relevant for the present study, *Yeo and Kim [2013]* find that with a 2 year CSEOF decomposition of 140 years of monthly SST from the Extended Reconstruction SST v3 [*Smith et al., 2008*] data set, two dominant global modes of variability focused primarily in the tropical Pacific were obtained and subsequently related to the SO. This same analysis is repeated here with the resulting LVs and PCTS for the first two modes shown in Figure 1. These two modes are referred to hereafter as the first and second modes, but it should be noted that these are the dominant two modes only after removing the global trend and seasonal signal. The first mode shown on the left of Figure 1 describes low-frequency variability in the Pacific Ocean, likely signifying a link between the tropical Pacific and northern Pacific on interannual to decadal timescales. There is strong variability in the central and eastern north Pacific, with the spatial pattern

showing a similar structure to the Pacific Decadal Oscillation (PDO) [Mantua *et al.*, 1997; Mantua and Hare, 2002]. The PCTS of this mode shows a strong correlation of  $r^2 = 0.80$  with a 2 year moving-average of the monthly PDO index over the time period from 1950 to present, i.e., the time period of interest for this study. Several studies have recently suggested that the low-frequency variability of the SO is modulated by decadal variability (PDO) in the north Pacific [Gu and Philander, 1997; Latif *et al.*, 1997; Barnett *et al.*, 1999; Kleeman *et al.*, 1999; Pierce *et al.*, 2000; Vimont *et al.*, 2003]. As discussed in Yeo and Kim [2013], this mode likely represents the link between the tropical Pacific and the North Pacific—and by extension the link between the SO and the PDO—on longer timescales. While the argument could be made that this mode should be referred to as the PDO, for the purposes of this paper and for ease of discussion, this mode is referred to as an ENSO mode and should be understood as a representation of the low-frequency variability of the SO. The second CSEOF mode represents the biennial oscillation of the SO with the LV capturing the phase transition between WE and CE. As expected, the maximum amplitude is found at the end of the calendar year, with the preceding months demonstrating the build-up to the WE and CE. The PCTS clearly shows the strong ENSO events in 1972/1973, 1982/1983, and 1997/1998. Note that the signs for the 1972/1973 WE and 1982/1983 WE are negative in the PCTS as it begins on an odd year rather than an even year, an artifact of the 2 year nested period. In other words, the odd years correspond to year 1 of the modes in Figure 1, while the even years correspond to year 2 of the modes shown in the figure.

#### 4. CSEOF Analysis of NCEP/NCAR Reanalysis SLP

To isolate the variability associated with the SO in the Southern Hemisphere, CSEOF analysis is applied to the monthly averaged NCEP/NCAR Reanalysis SLP spanning the time period from January 1948 to July 2014 using a 2 year nested period. With this shorter record, however, it becomes difficult to separate out the low-frequency SO mode from the biennial oscillation SO mode, both of which are likely important to the description of the onset of SO extreme events. To remedy this problem, we rely on CSEOF regression analysis (demonstrated in, for example, Yeo and Kim [2013]) that allows us to obtain CSEOF SLP modes that are physically consistent with corresponding CSEOF SST modes. More specifically, the regression analysis allows for the creation of regressed SLP CSEOF LVs that have the same temporal evolution (PCTS) as the two SST modes shown in Figure 1. Although the regression forces the LVs to have the same (or similar) PCTS, it does not dictate that the resulting LVs be in phase. On the contrary, the phase information of the LVs is built into the analysis through this regression, a significant advantage over other analysis/decomposition techniques. The CSEOF regression technique provides a straightforward way of determining lead-lag relationships between different variables, which is a motivation for using it here. The resulting set of LVs are said to be physically consistent and, assuming a regression relationship can be established, are analyzed in tandem to gain information about the signal or system of interest. The following steps outline the procedure for obtaining LVs in one variable (in this case, SLP; predictor, labeled with subscript P) that have the same PCTS of another variable (in this case, SST; target, labeled with subscript T):

1. Perform CSEOF decompositions of the target variable and the predictor variable over a common time period.
2. Regress all predictor PCTS (in this study,  $i = 20$ ) on each individual target PCTS ( $n = 2$  in present study for the two modes shown in Figure 1), to compute a set of regression coefficients,  $\alpha$ :

$$PCTS_{T,n}(t) = \sum_i \alpha_{i,n} PCTS_T(t) + \varepsilon_n(t) \quad (2)$$

3. Use the regression coefficients computed in (2), along with the original predictor loading vectors,  $LV_P$ , to form the predictor variable spatial patterns,  $LVR_P(r, t)$ , with amplitude fluctuations described by  $PCTS_T(t)$ :

$$LVR_{P,n}(r, t) = \sum \alpha_{i,n} LV_{P,i}(r, t) \quad (3)$$

Leveraging the CSEOF result from SST shown in Figure 1 and using this regression technique, physically consistent SLP modes explaining the lower and higher frequency components of the SO are extracted. We first perform a CSEOF decomposition of the SLP data in the domain from 100°E to 60°W and 50°S to 40°N. After regressing onto the two SST modes in Figure 1, the subsequent regressed CSEOF SLP modes are shown

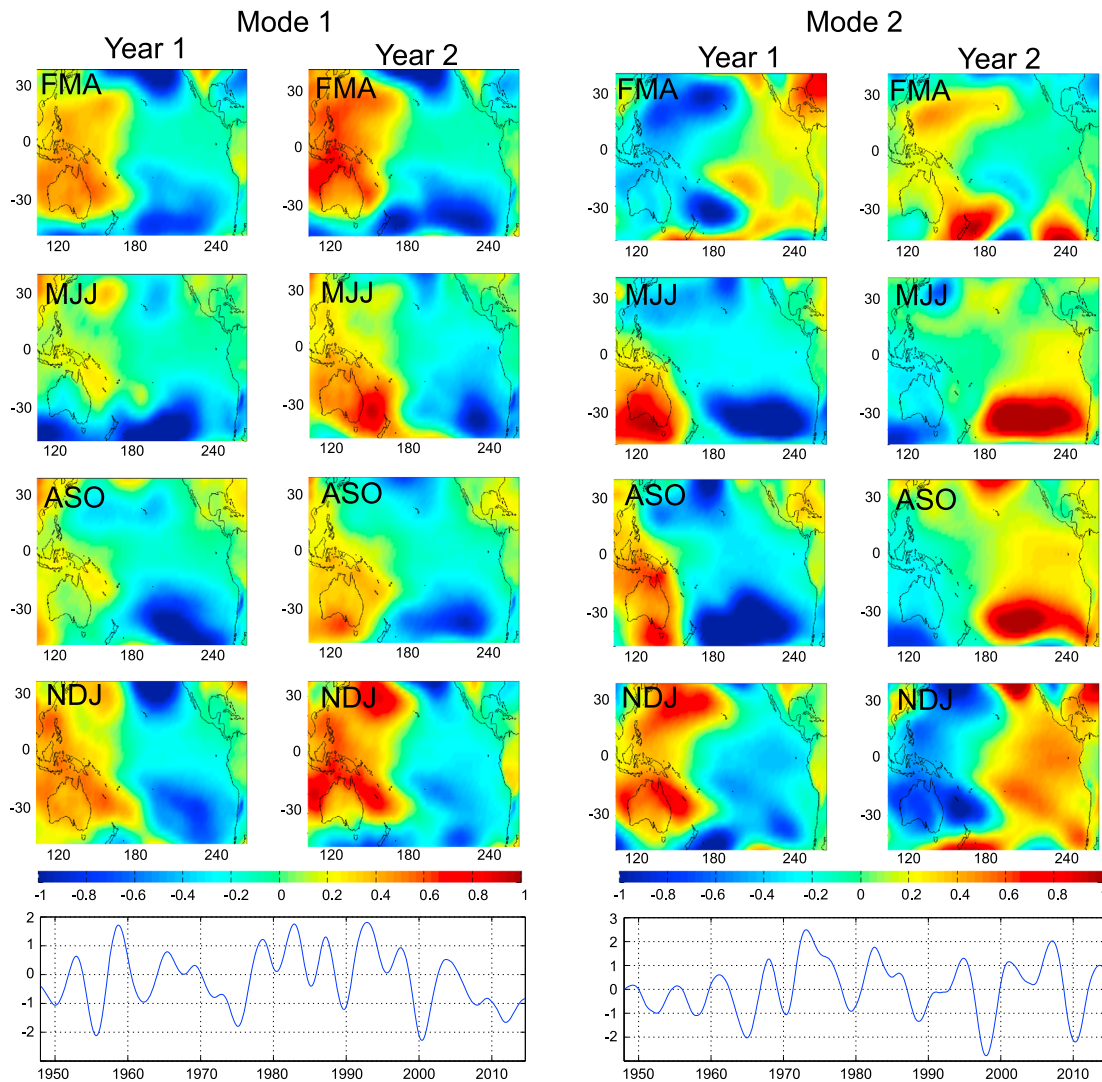


**Figure 2.** (left) SLP CSEOF Mode 1 from NCEP-NCAR Reanalysis data, representing low frequency variability associated with the SO. (top) LVs and (bottom) PCTS are shown (units: mb). (right) SLP CSEOF Mode 2 of the CSEOF decomposition representing the biennial oscillation between warm and cold SO events (unit: mb).

in Figure 2, with the low frequency SO mode on the left, and the mode describing the biennial oscillation between CE and WE on the right. Note that since the decomposition and analysis of the data begins in 1948, the even years correspond to year 1 of the modes in Figure 2, while the odd years correspond to year 2 of the modes shown in the figure. Given the low frequency nature of the mode (Figure 2, left), many of the features are stationary, with a strong anomalous high over Australia and anomalous low in the central and eastern Southern Hemisphere present throughout the two year nested period. The PCTS (bottom left panel of Figure 2) has a high correlation ( $r^2 = 0.80$ ) with the Pacific Decadal Oscillation (PDO) [Mantua *et al.*, 1997; Mantua and Hare, 2002] index, with the phase transition in 1976/1977 evident in the time series. The second mode, related to the biennial oscillation of the SO, captures the transition between WE and CE. In year 1 of mode 2, the anomalous high sets up over Australia in MJJ, with an anomalous low found east of New Zealand. In year 2, the high over Australia dissipates and becomes an anomalous low, suggesting the transition from a WE to a CE. It is important to note that there are different times when modes 1 and 2 combine constructively or destructively. When mode 1 is in phase with mode 2, the high over Australia can be greatly strengthened through the combination of the two modes. This could then lead to a stronger than usual WE. Conversely, when the two are out of phase, mode 1 could act destructively to limit the strength of a building warm or cold event.

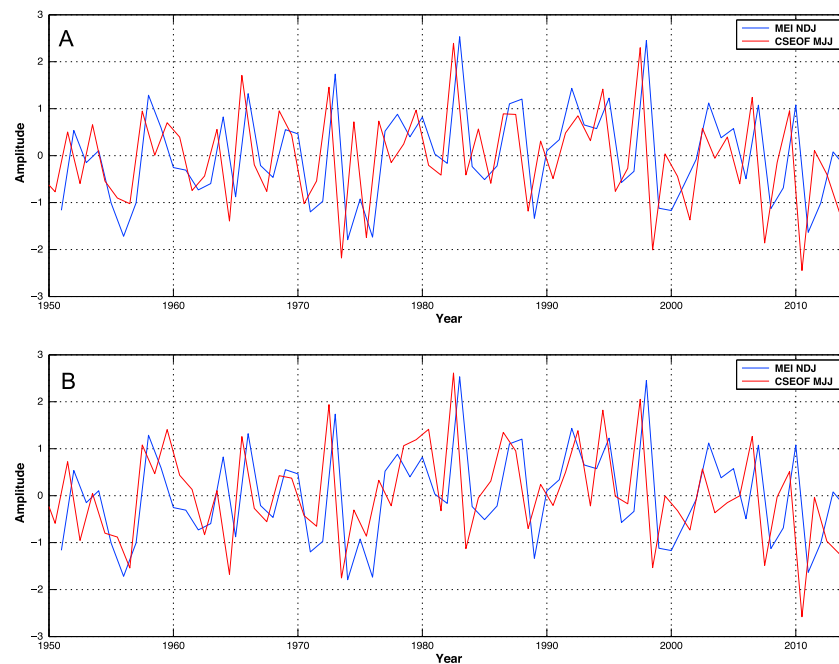


**Figure 3.** From NCEP-NCAR data, May-June-July (MJJ) SLP area-averages (red) taken over the region from 15°S to 45°S and 180°W to 90°W, and compared to the November-December-January (NDJ) of Multivariate ENSO Index (MEI, blue). Area-averages are computed from (a) combined CSEOF modes 1 and 2, 2 year nested period, and (b) area-average for a near real time (NRT) precursor obtained by projecting LV maps from February to July for both modes 1 and 2 on to original data. Note that sign is reversed on the area-averages for easier comparison to MEI.

## 5. ENSO WE and CE Precursor

By separating the SO SLP variability in the Southern Hemisphere into two CSEOF modes, it is possible to gain a better understanding of the evolution of the SO and develop a precursor that could be tracked in near real time (NRT) providing an accurate contributor in prediction models for the onset of WE and CE. Using the combined variability from CSEOF modes shown in Figure 2, MJJ averages are computed and compared to the November-December-January (NDJ) values of the Multivariate ENSO Index (MEI) [Wolter and Timlin, 2011]. Averages are taken over the region from 15°S to 45°S and 180°W to 90°W. This region spans the climatological position of the subtropical high-pressure system to the east of New Zealand and offshore of South America. So, for WE the SLP values are negative corresponding to a weaker subtropical high, while for CE the SLP values are positive (stronger high-pressure system). Figure 3a shows the MJJ value for the combined contribution of regressed modes 1 and 2 given in Figure 2.

As a consequence of the nested period in the CSEOF analysis, there is added uncertainty in the values at the end of the PCTS due to boundary effects. As it relates to this study, it is important to accurately know the relative strengths of modes 1 and 2 as close to the present as possible in order to establish a usable precursor. To both check the PCTS values at the end of the record and establish a procedure for computing the precursor in NRT, the spatial patterns for February through July for modes 1 and 2 are projected on to the original SLP data before computing the area-average as discussed above. CSEOF modes are not orthogonal at each point in time; rather the orthogonality spans the entire nested period. In order to project the two modes simultaneously, a time period within the nested period must be selected when the modes have near-zero correlation. Importantly, the correlation of the LVs for modes 1 and 2 between February-July is 0.11 in year 1 and 0.15 in year 2. The resulting precursor after performing the projection is shown in Figure 3b (scaled by multiplying by MJJ average value) and again compared to the MEI to demonstrate the strong correlation. The agreement between this precursor time series and the MJJ time series computed directly from the CSEOF modes (Figure 3b) leads to a number of conclusions: (1) the values of the PCTS near the boundary accurately reflect the relative strength of the two modes in the actual data, (2) the precursor can be computed and updated without performing a full CSEOF analysis each time, and (3) the

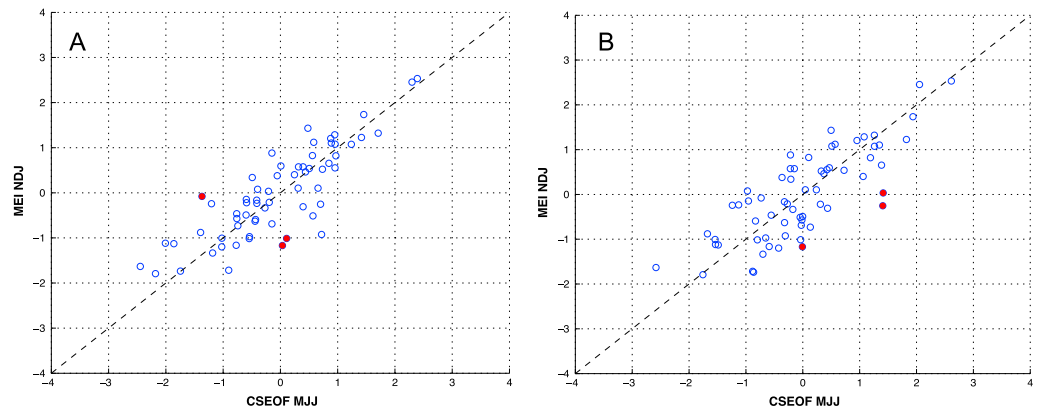


**Figure 4.** Scatter plots using NCEP-NCAR reanalysis data comparing NDJ value of MEI to MJJ value from (a) combined CSEOF modes 1 and 2 and (b) area-average for a near real time (NRT) precursor obtained by projecting LV maps from February to July for both modes 1 and 2 onto original data. Red points mark events when either the MEI NDJ value or CSEOF MJJ value was both greater than 1 and had a difference between the two values of greater than 1.

evolution of the SLP in the Southern Hemisphere in the months (FMA) before MJJ is important and relevant to the development and onset of WE and CE, further confirming the dynamical description outlined above. By relying on the information gained from the CSEOF analysis of the full record, this projection technique paves the way for the precursor to be computed as data becomes available (in NRT) with the potential to be useful even before the middle of the year.

To better evaluate the skill of the precursor, scatter plots are computed to more clearly visualize the relationship between the MJJ SLP variability and the subsequent NDJ ENSO. Figure 4a shows the comparison between the NDJ value of MEI and the area-average MJJ value from the combined regressed SLP CSEOF modes 1 and 2. The comparison between the MEI NDJ and The area-average for a near real time (NRT) precursor obtained by projecting LV maps from February to July for both modes 1 and 2 onto original data is shown in Figure 4b. Events when either the MEI NDJ value or CSEOF MJJ value were both greater than one and had a difference between the two values of greater than one are marked in red. These marked events are considered to be extreme failures, when the SLP variability in MJJ serves to vastly underestimate or overestimate the potential for an extreme event in NDJ. While there are relatively few failures, future work will investigate whether these failures have a dynamical explanation or are simply a result of deficiencies in the data and/or analysis techniques.

In general, the MJJ Southern Hemisphere SLP serves as an excellent precursor (both in terms of occurrence and magnitude) for a WE or CE arising in NDJ. The spread for CE, however, appears larger than that for WE, suggesting better relation between MJJ SLP variability and the development of a WE. This could be related to the short record length of the original data, or—as discussed in the introduction—the view that the evolution toward a WE and the evolution toward a CE are not exactly mirror image processes. Additionally, while the NRT precursor (Figure 4b) is largely successful in forecasting extreme events, the spread is generally larger when compared to Figure 4a that shows the MJJ SLP values calculated directly from the CSEOF modes. As a measure of this, the mean squared error relative to the MEI is 0.33 for the CSEOF modes (Figure 4a) and 0.42 for the NRT precursor (Figure 4b). This highlights that while the variability described by the CSEOF modes is clearly important in the onset of WE and CE, further work may be needed to extend this description to the creation of a NRT precursor, including analysis of how best to relate the information in the CSEOF modes to the NRT measurements.

As an additional test of the precursor, the length of time series used to create the basis function was varied. This test served two purposes: (1) to determine if the record length of NCEP/NCAR reanalysis data (60+ years) is potentially hindering the ability to separate the low-frequency ENSO variability from the biennial ENSO variability and (2) to determine if the NRT precursor can successfully forecast events that occur outside of the period over which the basis functions are calculated. Starting at 20 years (from 1948 to 1967) and incrementing by 5 years up to 65, regressed CSEOF modes were computed from the shortened record and subsequently used as a NRT precursor – as described above—to forecast WE and CE over the full record



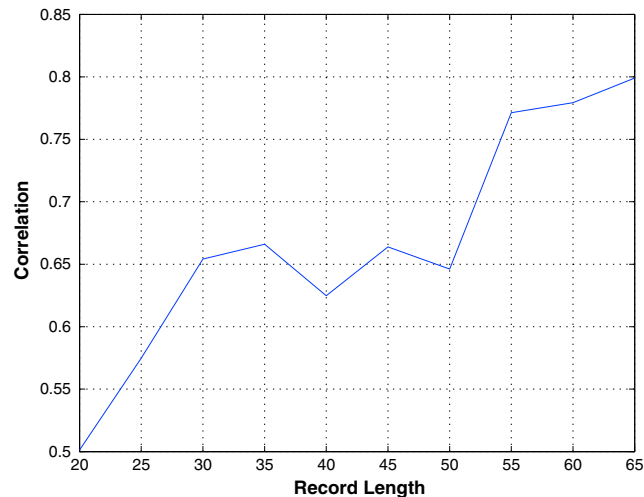


**Figure 5.** Correlation between time series of MEI NDJ values and CSEOF precursor MJJ values as function of record length used to compute the CSEOF basis functions. Correlations are computed using the NCEP-NCAR reanalysis data from 1950 to 2014.

from 1948 to 2014. As shown in Figure 5, as expected, the agreement between the MJJ value estimated from the precursor and the NDJ value of the MEI improves significantly from 20 years to 55 years before leveling off. This test does not necessarily accurately reflect the ability or skill of this precursor, however, since in practice, the basis functions would be recomputed frequently. This precludes the possibility of using basis functions computed more than a year before the event that is being forecast. Nevertheless, this result suggests that almost the full record of the NCEP/NCAR data set is required to successfully forecast WEs and CEs, and that further improvement may be seen with the use of a longer SLP record.

## 6. CSEOF Analysis of HadSLP2 SLP

The Met Office Hadley Centre's mean SLP data set, HadSLP2, provides a long historical record of SLP from 1850 to 2005. The data set was created using marine observations from ICOADS and land observations from 2228 stations around the globe. The land and marine observations were blended and the pressures were reconstructed using a reduced-space optimal procedure. While the record is much longer than the NCEP/NCAR reanalysis SLP, the data are provided on a coarse  $5^\circ$  resolution grid and has not been extended to present using a consistent computation technique over the full record. Nevertheless, the data set provides the opportunity to gauge the improvement gained in forecasting WEs and CEs using a longer record for computing the basis functions.

As a first step, a 2 year CSEOF decomposition of the HadSLP2 data was performed from 1850 to 2005. The first two ENSO-related modes more clearly exhibited the low-frequency variability and biennial frequency than the comparable modes from the NCEP/NCAR data. Without performing the regression, the correlation coefficients between the two SST modes shown in Figure 1 and the corresponding HadSLP2 modes was found to be 0.83 and 0.86, respectively, demonstrating greatly improved separation of the two modes of ENSO variability when compared to the shorter NCEP/NCAR record. While perhaps not necessary given the high correlations, we still perform the CSEOF regression to obtain SLP modes from the HadSLP2 with the same PCTS as those in the SST modes shown in Figure 1. This also provided the opportunity to make a direct comparison to the two regressed modes from the NCEP/NCAR data. The resulting regressed CSEOF modes are shown in Figure 6. When comparing the modes in Figures 2 and 6, one of the most notable differences is found in the low-frequency ENSO mode. With the longer HadSLP2 data, the anomalous high over Australia and anomalous low east of New Zealand are persistent throughout the year, not exhibiting the weakened signal in MJJ and ASO visible in Figure 2. This is consistent with the corresponding SST mode shown in Figure 1 that does not vary significantly over the 2 year nested period. The biennial oscillation mode is not substantially different between the two SLP data sets, suggesting the shorter NCEP/NCAR record is long enough to capture the higher frequency portion of ENSO variability. The signal in the HadSLP2 data set is roughly half the size of the signal in the NCEP/NCAR data set (note the different color bar scales in Figures 2 and 6). As a check and to determine the relative importance of the two regressed modes in each data set, the percent of variance explained by the combined modes was calculated (Figure 7). The two modes explain slightly more of the variance in the NCEP/NCAR data set, but the modes are still dominant in the HadSLP2 data set, explaining greater than 40% of the variance (once the seasonal signal is removed) in large part of the domain. Additionally, the fact that the CSEOF analysis of the HadSLP2 without the addition of the regression yielded two dominant SLP modes closely related to the SST modes in Figure 1 highlights the importance of this signal with regards to the overall SLP variability in the Southern Hemisphere.

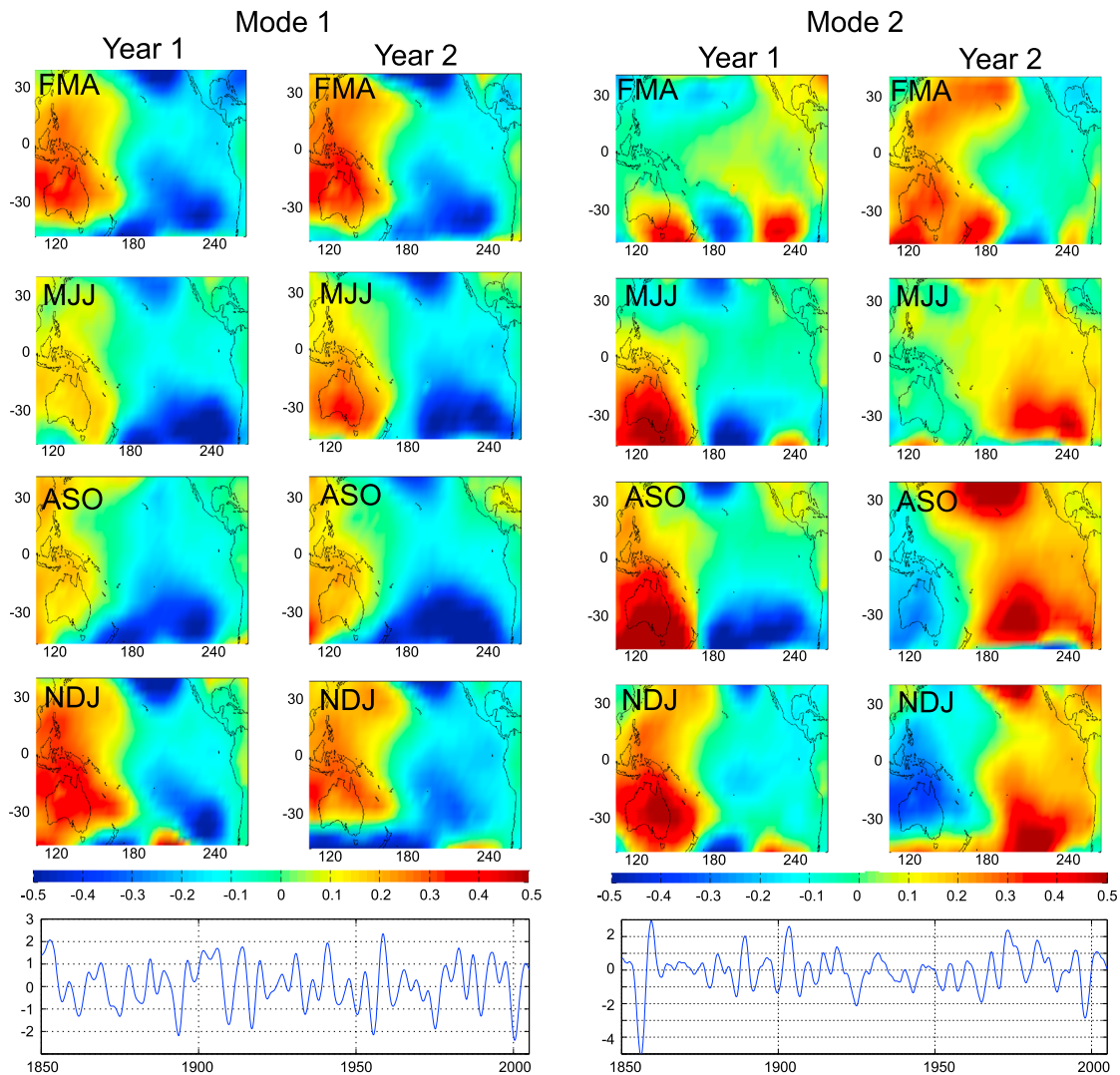


**Figure 6.** (left) SLP CSEOF Mode 1 from HadSLP2 data, representing low frequency variability associated with the SO (unit: mb). (top) LVs and (bottom) PCTS are shown. (right) SLP CSEOF Mode 2 of the CSEOF decomposition representing the biennial oscillation between warm and cold SO events (unit: mb).

As was done for the NCEP/NCAR data, we compared the MJJ-signal from the HadSLP2 regressed CSEOF modes to NDJ of the MEI (note, the extended version of the MEI is used for this comparison). MJJ SLP area-averages were again taken over the region from 15°S to 45°S and 180°W to 90°W, and compared to the NDJ of the MEI. Area-averages were computed from the combined CSEOF modes 1 and 2 (Figure 8a), and for the NRT precursor obtained by projecting LV maps from February to July for both modes 1 and 2 on to original data (Figure 8b). With the HadSLP2 data set, we are able to examine the relationship between MJJ SLP and the ENSO development in NDJ over a much longer record. While the relationship appears to hold (qualitatively) throughout the record, scatter plots are created to assess the precursor mode carefully. Figure 9 shows the MJJ value plotted versus the NDJ MEI value for the combined CSEOF modes (Figure 9a; 0.26 mean squared error relative to MEI) and for the NRT precursor (Figure 9b; 0.43 mean squared error relative to MEI). For the combined modes, the relationship between MJJ SLP and the NDJ ENSO signal appears to be improved for CEs, in particular, when compared to the NCEP/NCAR data shown in Figure 4a. The precursor computed from the HadSLP2 data also performs comparably to the NCEP/NCAR precursor with 8 failures (versus 3 failures for NCEP/NCAR), which is consistent with the roughly 2.5 times longer record. The majority of these failures (5) occurred before 1940.

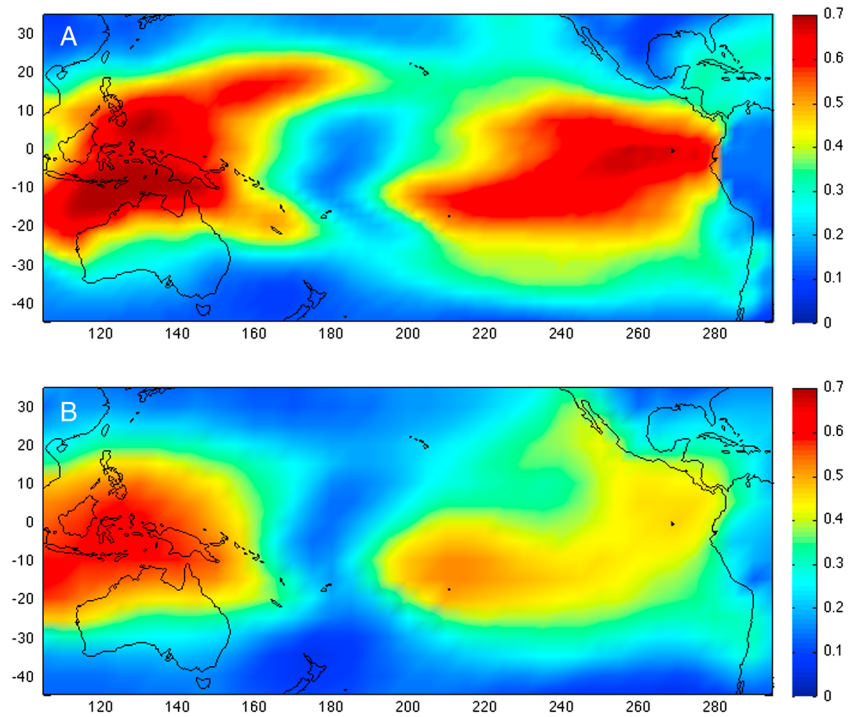


**Figure 7.** Variance of original data (after the seasonal signal is removed) explained by combined CSEOF modes 1 and 2 for (a) NCEP-NCAR data and (b) HadSLP2 data. Maximum and minimum possible values are 1 and 0, respectively.

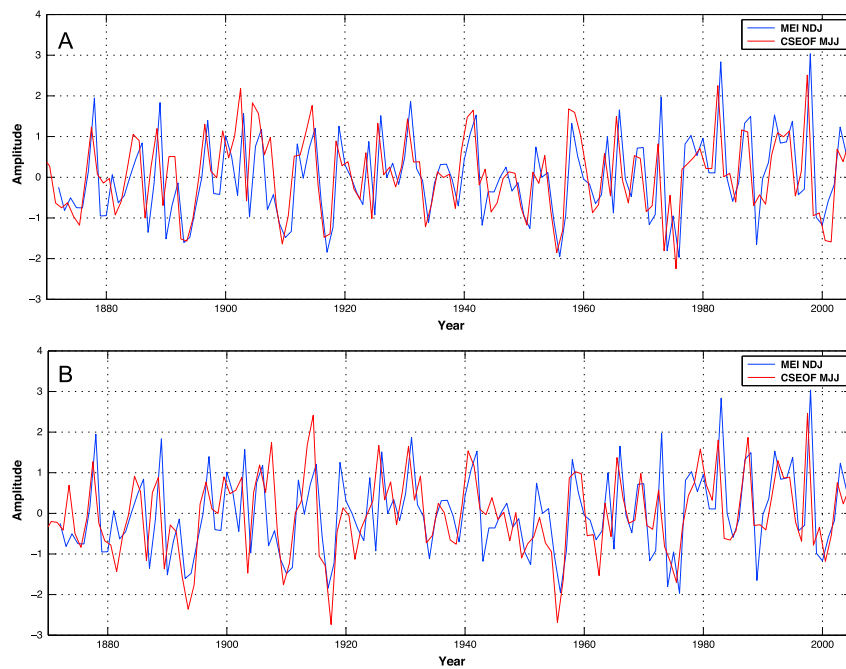


**Figure 8.** From HadSLP2 data, May-June-July (MJJ) SLP area-averages (red) taken over the region from 15°S to 45°S and 180°W to 90°W, and compared to the November-December-January (NDJ) of Multivariate ENSO Index (MEI, blue). Area-averages are computed from (a) combined CSEOF modes 1 and 2, 2 year nested period, and (b) area-average for a near real time (NRT) precursor obtained by projecting LV maps from February to July for both modes 1 and 2 on to original data. Note that sign is reversed on the area-averages for easier comparison to MEI.

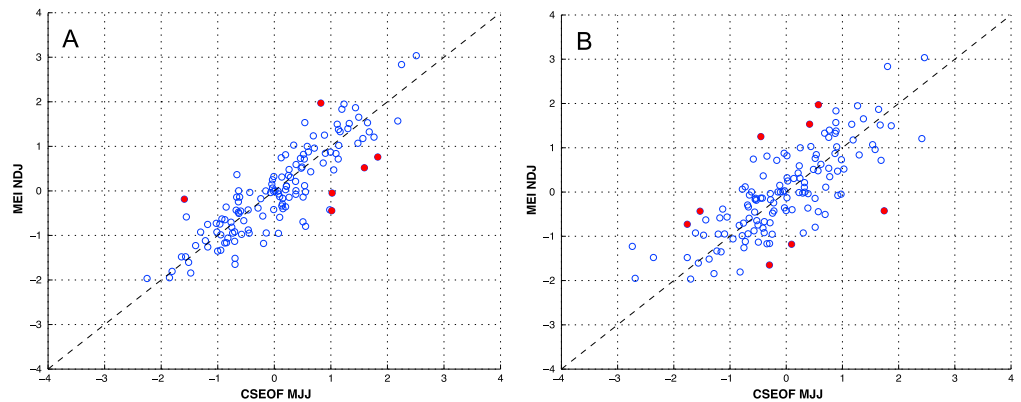


**Figure 9.** Scatter plots using HadSLP2 data comparing NDJ value of MEI to MJJ value from (a) combined CSEOF modes 1 and 2 and (b) area-average for a near real time (NRT) precursor obtained by projecting LV maps from February to July for both modes 1 and 2 on to original data. Red points mark events when either the MEI NDJ value or CSEOF MJJ value was both greater than 1 and had a difference between the two values of greater than 1.

## 7. Discussion

In the past several months, there has been much discussion regarding the possibility of a WE developing in the latter half of 2014. With the MJJ precursor isolated into a pair of CSEOF modes, it is possible to look at the conditions in the Southern Hemisphere preceding past WE in the full record and compare to the current state of the SO in the Southern Hemisphere. Figure 10 shows the combined contributions from CSEOF modes 1 and 2 for May, June, and July of 1972 (top), 1997 (middle), and 2014 (bottom; note that given the agreement between the values in Figures 3b and 3c, the PCTS is used directly to create the figure for 2014). While the 1997/1998 WE was the largest in the 60+ year record, the WE in 1972/1973 was of less exceptional strength and provides a good comparison for the SLP development of 2014. For the May, June, and July SLP of both 1972 and 1997, an anomalous high over Australia and an anomalous low off the east coast of New Zealand are clearly visible, describing the expected evolution of the SO discussed above in MJJ leading to a WE. In 2014, a weak high is seen in May and June but dissipates in July. This weak high is also found south of Australia, a significant departure in location when compared to the other two WE. Furthermore, there is little sign of an anomalous low in the central Pacific midlatitudes that would drive southerly flow toward the equator. Based on these maps and the small values for the precursor shown in Figure 3, it is unlikely that a WE will develop and instead points to neutral-to-slightly positive conditions in the eastern equatorial Pacific for the latter half of 2014 and beginning of 2015. As discussed above, when the low-frequency mode is in phase with biennial oscillation mode, the high over Australia can be greatly strengthened through the combination of the two modes. This could then lead to a stronger than usual WE. Conversely, when the two are out of phase, the low-frequency mode could act destructively to limit the strength of a building warm or cold event. This appears to be the case for the 2014 WE that failed to develop and increase in strength. Based on the analysis here, the phase of the low-frequency mode (and by extension the PDO) did not support the development of a strong WE in 2014.

Forecasting warm and cold extremes of the ENSO has largely focused on the equatorial Pacific SST, and little has been done to incorporate information from the Southern Hemisphere to improve predictions of the onset and development of extreme events. Furthermore, prior to this study, the dynamics of the SLP in the Southern Hemisphere preceding a WE or CE had been described using anomaly values and without relying on modal analyses [e.g., *van Loon et al.*, 2003; *Stephens et al.*, 2007]. By using CSEOF analysis to extract a similar dynamical description to that provided in those previous studies in two CSEOF modes, we demonstrate how significant these dynamics are with regard to the total variability of the Southern Hemisphere and equatorial region in the Pacific. The separation of SO variability into two modes—one for the low-frequency signal and one for the biennial oscillation—also leads to an improved understanding of how the SLP development can lead to a warm or cold extreme event. In particular, to obtain a large WE or CE, the two modes must combine constructively with the low-frequency high over Australia seen in mode 1 aligning with the anomalous high over Australia visible in the biennial oscillation described in mode 2. When neither mode is strongly present—as in MJJ of 2014—a WE (or similarly a CE) is unlikely.

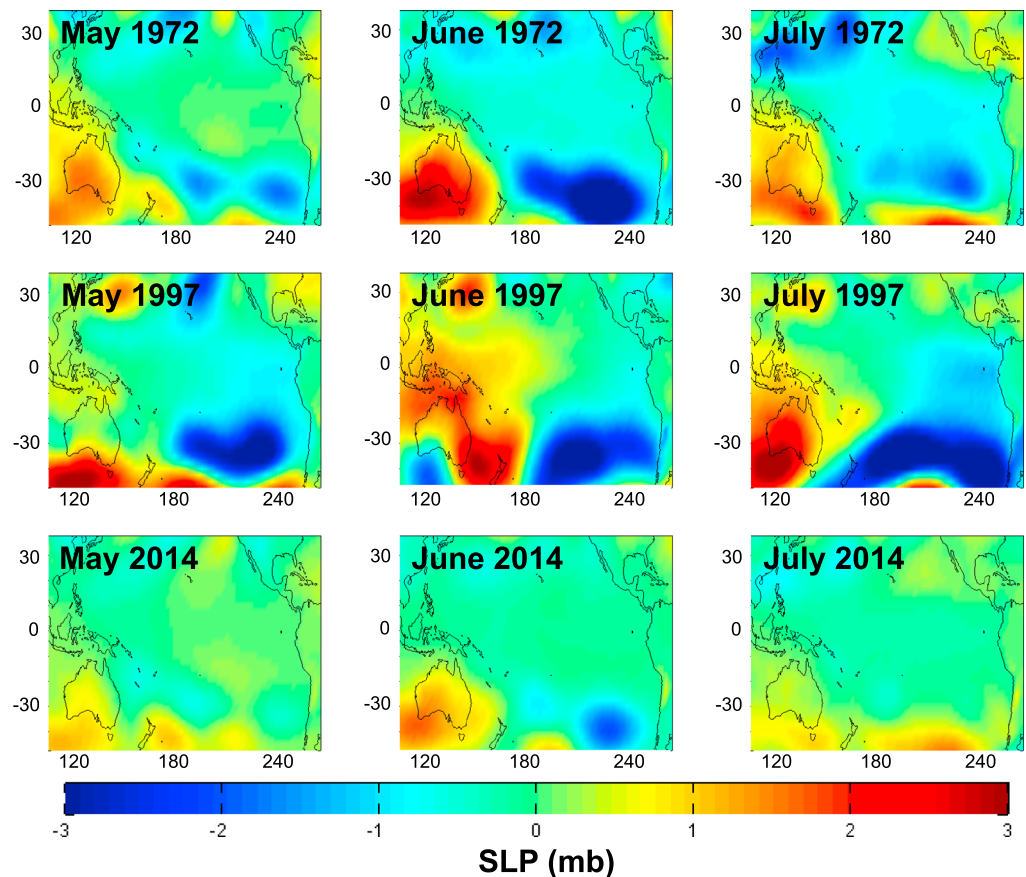


**Figure 10.** Using NCEP-NCAR reanalysis data, combined SLP contribution from modes 1 and 2 for May, June, and July of (top) 1972, (middle) 1997, and (bottom) 2014.

CSEOF analysis provides a powerful tool for extracting such signals, relying on the physical periods inherent to SO variability and known to be present in the SLP data. Furthermore, CSEOF analysis allows for the isolation of the MJJ precursor, providing a reliable metric for assessing the likelihood of an impending warm or cold event. The CSEOF-derived MJJ precursors shown in Figures 3 and 8 demonstrate an improved ability to separate the variability associated with an impending extreme event when compared to MJJ precursor metrics computed from anomaly SLP data. The analysis presented herein demonstrates that SLP variations in MJJ are strong predictors for the peak warming (or cooling) of tropical eastern Pacific SST that mark the mature phase of a WE (or CE) in November and December (year<sub>0</sub>), and through January of the following year (year<sub>+1</sub>). This analysis also provides two specific modes of variability that can be tracked in near real time to assess the onset and development of ENSO events and form the foundation of a precursor that can be used to supplement and/or verify forecasts arising from other techniques.

#### Acknowledgments

B. D. H. acknowledges support from NASA ROSES grant NNX13AH05G. R. F. M. acknowledges support from a NASA OWWST grant. K. Y. K. acknowledges support by the project entitled "Ocean Climate Change: Analysis, Projections, Adaptation (OCCAPA)" funded by the Ministry of Land, Transport, and Maritime Affairs, Korea. The SLP data used here are freely available at <http://www.esrl.noaa.gov/psd/data/reanalysis/reanalysis.shtml>, while the SST data are freely available at <http://www.esrl.noaa.gov/psd/data/gridded/data.noaa.ersst.html>.

#### References

- Barnett, T. P., D. W. Pierce, M. Latif, D. Dommenget, and R. Saravanan (1999), Interdecadal interactions between the tropics and midlatitudes in the Pacific Basin, *Geophys. Res. Lett.*, *26*(5), 615–618.
- Bjerknes, J. A. (1966), Possible response of the atmospheric Hadley circulation to equatorial anomalies of ocean temperature, *Tellus*, *97*, 820–829.
- Bjerknes, J. A. (1969), Atmospheric teleconnections from the equatorial Pacific, *Mon. Weather Rev.*, *97*, 163–172.
- Chen, D., M. A. Cane, A. Kaplan, S. E. Zebiak, and D. Huang (2004), Predictability of El Niño over the past 148 years, *Nature*, *428*, 733–735.
- Gu, D., and S. G. Philander (1997), Interdecadal climate fluctuations that depend on exchanges between the tropics and extratropics, *Science*, *275*(5301), 805–807.
- Harrison, D. E., and N. K. Larkin (1996), The COADS sea level pressure signal: A near-global El Niño composite and time series view, 1946–1993, *J. Clim.*, *9*, 3025–3055.
- Hong, L.-C., LinHo, and F.-F. Jin (2014), A Southern Hemisphere booster of super El Niño, *Geophys. Res. Lett.*, *41*, 2142–2149, doi:10.1002/2014GL059370.

- Kerr, R. A. (2002), Signs of success in forecasting El Niño, *Science*, 297, 497–499.
- Kidson, J. W., and J. A. Renwick (2002), The Southern Hemisphere evolution of ENSO during 1981–99, *J. Clim.*, 15, 847–863.
- Kiladis, G. N., and H. van Loon (1988), The Southern Oscillation. Part VII: Meteorological anomalies over the Indian and Pacific sectors associated with the extremes of the oscillation, *Mon. Weather Rev.*, 116, 120–136.
- Kim, K.-Y. (2002), Investigation of ENSO variability using cyclostationary EOFs of observational data, *Meteorol. Atmos. Phys.*, 81(3), 149–168.
- Kim, K.-Y., and G. R. North (1997), EOFs of harmonizable cyclostationary processes, *J. Atmos. Sci.*, 54(19), 2416–2427.
- Kim, K.-Y., G. R. North, and J. Huang (1996), EOFs of one-dimensional cyclostationary time series: Computations, examples, and stochastic modeling, *J. Atmos. Sci.*, 53(7), 1007–1017.
- Kleeman, R., J. McCreary, and B. Klinger (1999), A mechanism for generating ENSO decadal variability, *Geophys. Res. Lett.*, 26(12), 1743–1746.
- Landsea, C. W., and J. A. Knaff (2000), How much skill was there in forecasting the very strong 1997–98 El Niño?, *Bull. Am. Meteorol. Soc.*, 81, 2107–2119.
- Larkin, N. K., and D. E. Harrison (2002), ENSO warm (El Niño) and cold (La Niña) event life cycles: Ocean surface anomaly patterns, their symmetries, asymmetries, and implications, *J. Clim.*, 15, 1118–1140.
- Latif, M., R. Kleeman, and C. Eckert (1997), Greenhouse warming, decadal variability, or El Niño? An attempt to understand the anomalous, *J. Clim.*, 10(9), 2221–2239.
- Latif, M., D. Anderson, T. Barnett, M. Cane, R. Kleeman, A. Leetmaa, J. O'Brien, A. Rosati, and E. Schneider (1998), A review of the predictability and prediction of ENSO, *J. Geophys. Res.*, 103(C7), 14,375–14,393, doi:10.1029/97JC03413.
- Mantua, N. J., and S. R. Hare (2002), The Pacific Decadal Oscillation, *J. Oceanogr.*, 58, 35–44.
- Mantua, N. J., S. R. Hare, Y. Zhang, J. M. Wallace, and R. C. Francis (1997), A Pacific interdecadal climate oscillation with impacts on salmon production, *Bull. Am. Meteorol. Soc.*, 78, 1069–1079.
- Milliff, R. F., H. van Loon, and J. Brown (2009), Using the SVW climate data record to validate aspects of the southern oscillation, paper presented to the Ocean Vector Winds Science Team Special Meeting on “Scatterometers in Climate”, 20 pp., Arlington, Va.
- Pierce, D. W., T. P. Barnett, and M. Latif (2000), Connections between the Pacific Ocean tropics and midlatitudes on decadal timescales, *J. Clim.*, 13(6), 1173–1194.
- Rasmusson, E. M., and T. H. Carpenter (1982), Variations in tropical sea surface temperature and surface wind fields associated with the Southern Oscillation/El Niño, *Mon. Weather Rev.*, 110, 354–384.
- Rasmusson, E. M., X. Wang, and C. F. Ropelewski (1990), The biennial component of ENSO variability, *J. Mar. Syst.*, 1(1), 71–96.
- Smith, T. M., R. W. Reynolds, T. C. Peterson, and J. Lawrimore (2008), Improvements NOAA's historical merged land-ocean temp analysis (1880–2006), *J. Clim.*, 21, 2283–2296.
- Stephens, D. J., M. J. Meuleners, H. van Loon, M. H. Lamond, and N. P. Telcik (2007), Differences in atmospheric circulation between the development of weak and strong warm events in the Southern Oscillation, *J. Clim.*, 20, 2191–2209.
- van Loon, H. (1967), The half-yearly oscillations in middle and high southern latitudes and the coreless winter, *J. Atmos. Sci.*, 24, 472–486.
- van Loon, H. (1984), The Southern Oscillation. Part III: Associations with the trades and with the trough in the westerlies of the South Pacific Ocean, *Mon. Weather Rev.*, 112, 947–954.
- van Loon, H., and R. A. Madden (1981), The Southern Oscillation. Part I: Global associations with pressure and temperature in northern winter, *Mon. Weather Rev.*, 109, 1150–1162.
- van Loon, H., and D. J. Shea (1985), The Southern Oscillation. Part IV: The precursors south of 15S to the extremes of the oscillation, *Mon. Weather Rev.*, 113, 2063–2074.
- van Loon, H., and D. J. Shea (1987), The Southern Oscillation. Part VI: Anomalies of sea level pressure on the Southern Hemisphere and of Pacific sea surface temperature during the development of a warm event, *Mon. Weather Rev.*, 115, 370–379.
- van Loon, H., G. A. Meehl, and R. F. Milliff (2003), The Southern Oscillation in the early 1990s, *Geophys. Res. Lett.*, 30(9), 1478, doi:10.1029/2002GL016307.
- Vimont, D. J., J. M. Wallace, and D. S. Battisti (2003), The seasonal footprinting mechanism in the Pacific: Implications for ENSO, *J. Clim.*, 16, 2668–2675.
- Wolter, K., and M. S. Timlin (2011), El Niño/Southern Oscillation behavior since 1871 as diagnosed in an extended multivariate ENSO index (MEI.ext), *Int. J. Climatol.*, 31, 1074–1087.
- Yeo, S.-R., and K.-Y. Kim (2013), Global warming, low-frequency variability and biennial oscillation: An attempt to understand the physical mechanisms driving major ENSO events, *Clim. Dyn.*, doi:10.1007/s00382-013-1862-1.